Arabian Journal of Chemistry (2021) **14**, 103052

King Saud University

Arabian Journal of Chemistry

www.ksu.edu.sa
www.sciencedirect.com

ORIGINAL ARTICLE

A water-stable functionalized NiCo-LDH/MOF nanocomposite: green synthesis, characterization, and its environmental application for heavy metals adsorption

Roozbeh Soltani [a], **Rasool Pelalak** [b,c], **Mahboubeh Pishnamazi** [b,d], **Azam Marjani** [e,f,*], **Saeed Shirazian** [g,h]

[a] *Department of Chemistry, Islamic Azad University, Arak Branch, Arak, Iran*
[b] *Institute of Research and Development, Duy Tan University, Da Nang 550000, Viet Nam*
[c] *Faculty of Environmental and Chemical Engineering, Duy Tan University, Da Nang 550000, Viet Nam*
[d] *Faculty of Pharmacy, Duy Tan University, Da Nang 550000, Viet Nam*
[e] *Department for Management of Science and Technology Development, Ton Duc Thang University, Ho Chi Minh City, Viet Nam*
[f] *Faculty of Applied Sciences, Ton Duc Thang University, Ho Chi Minh City, Viet Nam*
[g] *Department of Chemical Sciences, Bernal Institute, University of Limerick, Limerick, Ireland*
[h] *Laboratory of Computational Modeling of Drugs, South Ural State University, 76 Lenin prospekt, 454080 Chelyabinsk, Russia*

Received 1 December 2020; accepted 28 January 2021
Available online 3 February 2021

KEYWORDS

Adsorption;
Green synthesis;
Heavy metals;
Surface functionalization;
Layered double hydroxides;
Metal-organic frameworks

Abstract Removal of toxic heavy metals from aquatic environments has become a major concern due to environmental problems and the potential hazards and risks posed by them. Nowadays, the adsorption method as one of the most effective methods of removing pollutants has attracted increasing attention among chemists and environmental researchers. However, one of the challenges is to design and develop more effective adsorbents as well as to prepare them *via* greener and safer approaches. In line with these goals, a functionalized $Ni_{50}Co_{50}$-layered double hydroxide/UiO-66-(Zr)-$(COOH)_2$ nanocomposite (LDH/MOF NC) was prepared *via* a facile and ''green'' synthesis protocol and used as an effective adsorbent for removal of mercury and nickel cations from aqueous media. UiO-66-(Zr)-$(COOH)_2$ nanoparticles were *in situ* grown homogeneously over the surface of the functionalized two-dimensional ultrathin $Ni_{50}Co_{50}$-LDH sheets. A green organic-solvent-free route was used to prepare the LDH/MOF NC in which the water is used as a green solvent. The

* Corresponding author at: Ton Duc Thang University, Ho Chi Minh City, Viet Nam.
E-mail address: azam.marjani@tdtu.edu.vn (A. Marjani).
Peer review under responsibility of King Saud University.

Production and hosting by Elsevier

https://doi.org/10.1016/j.arabjc.2021.103052

adsorption performance of LDH/MOF NC for removal of Hg(II) and Ni(II) cations was studied and the influence of some experimental factors, such as solution pH, initial metal concentration, and contact time, on the adsorption process were investigated. The theoretical maximum adsorption capacities based on the Langmuir isotherm were found to be 509.8 mg g^{-1} and 441.0 mg g^{-1} for Hg(II) and Ni(II), respectively, under constant conditions. We believe that the facile and "green" synthesis method used in this work can be a starting point for the fabrication and development of similar composite materials for future works, especially for use in adsorption, extraction, catalysis, and drug delivery applications.

1. Introduction

Heavy metals are elements possessing specific gravity larger than 5.0 as well as atomic weights between 63.5 and 200.6. Because of the fast growth and development of industries such as metal plating, mining, pesticides, fertilizers, batteries, tanneries, etc., these metals discharge to the surface and ground waters. Many heavy metal ions including mercury, nickel, lead, cadmium, chromium, and thallium are recognized as toxic, mutagenic, and carcinogenic because unlike organic pollutants, heavy metals are not biodegradable and tend to accumulate in living organisms (Fu and Wang, 2011). Mercury is a neurotoxin that can seriously damage the central nervous system and also is a causative agent of various sorts of disorders such as reproductive, immunological, motor, cardiac, nephrological, and even genetic (Zahir et al., 2005). Nickel exceeding its critical level might cause serious problems including pulmonary fibrosis, skin dermatitis, renal edema, gastrointestinal distress, as well as various types of acute and chronic disorders in human beings such as lung and kidney disorders (Akhtar et al., 2004; Denkhaus and Salnikow, 2002). Accordingly, the removal of these heavy metals from aquatic environments has become a growing public health concern.

To date, various methods like adsorption, polymeric membranes, ion-exchange, chemical precipitation, reverse osmosis, and electrochemical treatment technologies, have been developed and used to remove toxic metals from effluents at different conditions (Bhattacharya et al., 2018; Azimi et al., 2017; Marjani et al., 2020; Soltani et al., 2020b). Among these well-developed removal processes, adsorption method has found more applications owing to its remarkable properties such as designability of the adsorbents, reusability of the adsorbents, lack of sludge problems, low energy consumption, easy and low-cost operation, and availability of starting materials (Soltani et al., 2020f; Soltani et al., 2020e; Soltani et al., 2019; Soltani et al., 2020d). In recent years, the great potential of nanomaterials, generally considered as materials with a pore size or particle size up to 100 nm, as nanoadsorbents for adsorption of a vast variety of adsorbate species has been reported (Khajeh et al., 2013; Soltani et al., 2020c; Soltani et al., 2019). Layered double hydroxides (LDHs) (He et al., 2018; Liang et al., 2013) and metal–organic frameworks (MOFs) (Wen et al., 2018; Feng et al., 2018) are two well-known groups of nanomaterials that possess unique properties and have received increasing attention in environmental applications, especially heavy metals adsorption, over the past decade. However, the use of LDHs and MOFs separately as an adsorbent, especially for heavy metals removal, is frequently restricted due to the low surface area of LDHs and the difficulty in separating MOFs nanoparticles from water. Recently, Soltani and co-workers (Soltani et al., 2021; Soltani et al., 2020a) have developed nanocomposites based on LDHs and MOFs (LDH/MOF NC) in which MOF nanocrystals are uniformly grown on LDH sheets. By using this approach, the surface area of LDH/MOF NC (due to the presence of MOF nanoparticles) increases relative to the surface area of pure LDH. Also, using this method, a composite with a larger particle size (micrometer size) than pure MOF nanocrystals (nanometer size) will be obtained, which in turn facilitates the process of separating the adsorbent from the aqueous medium. Due to the potential adsorption sites within these composite structures as well as their stability in aqueous media, these nanoporous materials are effective adsorbents for the removal of heavy metals from aqueous media.

In this work, in accordance with our previous studies (Soltani et al., 2021; Soltani et al., 2020a), a new LDH/MOF NC with homogeneously distributed MOF nanoparticles was synthesized *via* a "green" synthesis approach and utilized for adsorption of Hg(II) and Ni(II) heavy metals from aqueous media. For this purpose, a set of synthesis strategy was implemented in accordance with the following protocols:

(1) environmentally friendly preparation of $Ni_{50}Co_{50}$-LDH with ultrathin two-dimensional (2D) sheets.
(2) surface functionalization of the LDH with an appropriate silane coupling agent (SCA) for improving interactions between MOF nanoparticles and LDH surface.
(3) environmentally friendly synthesis of LDH/MOF NC in which water is used as a solvent for *in situ* growth of MOF nanoparticles (UiO-66-(Zr)-$(COOH)_2$) on the LDH surface.

To characterize the surface morphology, crystalline structure, and textural properties of LDH/MOF NC, several instrumental analyses were used. Furthermore, the removal efficiency of Hg(II) and Ni(II) ions from aqueous media by this adsorbent was investigated to evaluate the adsorption properties of LDH/MOF NC as an adsorbent.

2. Experimental

2.1. Materials

Nickel(II) nitrate hexahydrate [$Ni(NO_3)\cdot 6H_2O$] (≥98.5%), cobalt(II) nitrate hexahydrate [$Co(NO_3)_2\cdot 6H_2O$] (98%), mercury(II) chloride ($HgCl_2$, ≥99.5%), 1,2,4,5-benzenetetracarboxylic acid (pyromellitic acid, 96%), zirconium(IV) chloride

($ZrCl_4$, ≥99.9%), and 3-[2-(2-aminoethylamino)ethylamino]propyltrimethoxysilane (triamino silane coupling agent, TASCA, technical grade) were purchased from Sigma-Aldrich (Spain). Ethylene glycol (EG, ≥98.0%), acetone (≥99.8%), sodium hydroxide pellets (NaOH, 99%), and hydrochloric acid (HCl, 36%) were purchased from Merck (Darmstadt, Germany). Ethanol (absolute and 96%) was purchased from Dr. Mojallali (Dr. Mojallali Chemical Complex Co. Tehran, Iran). Double-distilled water was used in the synthesis of the samples and adsorption experiments. All chemicals were used without further purifications.

2.2. Synthesis method

2.2.1. Synthesis of the LDH ($Ni_{50}Co_{50}$-LDH)

$Ni_{50}Co_{50}$-LDH was prepared according to the method reported by Soltani and co-workers (Soltani et al., 2020a). A 1-L round-bottom glass flask equipped with a magnetic bar was charged with $Co(NO_3)_2{\cdot}6H_2O$ (37.5 mmol, 10.91 g), $Ni(NO_3)_2{\cdot}6H_2O$ (18.8 mmol, 5.46 g), and a mixture of EG/water (280 mL/112 mL). The mixture was stirred until the salts were completely dissolved. After fixing the temperature of the mixture at 90 °C, urea (281.3 mmol, 16.89 g) was added and the mixture was stirred under reflux. After 3 h the reaction mixture was cooled to room temperature and the product filtered off and washed several times with water and ethanol 96%. Finally, the resulting pale green powder of LDH sheets (very fine powder) was obtained after drying the filter cake at 60 °C for 24 h.

2.2.2. Synthesis of the COOH/TA-LDH (carboxylic/triamino-functionalized $Ni_{50}Co_{50}$-LDH)

The surface of the LDH was functionalized according to the following procedure: in a dry 250-mL round-bottom glass flask containing 60 mL ethanol, the pure LDH (1.00 g) and TASCA (13.2 mmol, 3.50 g) were added and ultrasonicated for 15 min followed by refluxing for 24 h under nitrogen atmosphere. Afterward, the reaction mixture was cooled to room temperature, Buchner-filtered, repeatedly washed with water and ethanol, and dried at 60 °C for 24 h to yield triamino-functionalized LDH (TA-LDH). Then, a 250-mL round-bottom flask was charged with the resulting TA-LDH, pyromellitic acid (1.6 mmol, 0.40 g), and absolute ethanol (60 mL) followed by ultrasonication for 15 min and refluxing at 160 °C for 12 h under stirring and nitrogen atmosphere. Subsequently, the reaction mixture was cooled to room temperature, filtered off, rinsed with water and ethanol 96%, and dried sequentially at 40 °C for 12 h and at 100 °C for 12 h to yield pure LDH-TA/COOH.

2.2.3. Synthesis of the MOF (UiO-66-(Zr)-$(COOH)_2$)

UiO-66-(Zr)-$(COOH)_2$ was prepared according to the procedure reported by Yang et al. (2013). A 100-mL round-bottom glass flask equipped with a reflux condenser and magnetic stirrer was charged with $ZrCl_4$ (10 mmol, 2.33 g), pyromellitic acid (17 mmol, 4.32 g), and water (50 mL). The mixture is stirred at room temperature until the $ZrCl_4$ and pyromellitic acid is completely dissolved and then heated under reflux (100 °C) under air atmosphere for 24 h. Subsequently, the obtained white gel was Buchner-filtered and repeatedly rinsed with DI water. Afterward, the resulting precipitate was then dispersed in water, and the mixture was heated under reflux for 16 h, followed by Buchner filtration, repeatedly washing with acetone, and oven-drying at 30 °C to yield pure UiO-66-(Zr)-$(COOH)_2$.

2.2.4. Synthesis of the LDH/MOF NC (COOH/TA-$Ni_{50}Co_{50}$-LDH/UiO-66(Zr)-$(COOH)_2$ nanocomposite)

A 250-mL round-bottom glass flask equipped with a reflux condenser and magnetic stirrer was charged with COOH/TA-LDH (1.0 g) and 100 mL water. The mixture was ultrasonicated for 15 min followed by adding pyromellitic acid (5.9 mmol, 1.5 g) and $ZrCl_4$ (3.4 mmol, 0.8 g). The mixture was stirred at room temperature for 5 min and ultrasonicated for another 15 min. Then, the mixture was stirred under reflux (100 °C) under air atmosphere for 24 h. Afterward, the resulting mixture was cooled to room temperature, Buchner-filtered, and thoroughly washed with water. The resulting precipitate was then dispersed in water and the mixture was stirred under reflux for 16 h, followed by Buchner filtration, washing with acetone, and oven-drying at 30 °C to yield pure LDH/MOF NC.

2.3. Characterization of the samples

The crystalline structure of the samples was determined by powder X-ray diffraction (XRD, AW-XDM300, Asenware, China) analysis. The functional groups in the powder samples were identified by Fourier transform infrared (FT-IR, Thermo Nicole, model AVATAR 370, USA) spectroscopy. Field emission scanning electron microscopy (FESEM, SIGMA HV, Zeiss, Germany) was used to observe the morphology of the samples. Nitrogen adsorption–desorption measurement at 77 K was conducted using a porosimetry analyzer (Belsorp-mini II, BEL, Japan) to analyze the pore structure and textural properties of the samples. A flame atomic absorption spectrometer (FAAS, PerkinElmer Model A300, Norwalk, USA) was used for the analysis of heavy metals concentrations in the solutions.

2.4. The batch adsorption experiments

Stock solutions of Hg(II) and Ni(II) (1000 mg L^{-1}) were prepared by dissolving an appropriate amount of $HgCl_2$ and $Ni(NO_3)_2{\cdot}6H_2O$ in double-distilled water. Metal solutions of different initial concentrations were prepared by dilution of the stock solutions. All batch adsorption experiments were carried out by adding a fixed amount of LDH/MOF NC (adsorbent dose (W) = 2.0 mg) into 50-mL screw-cap polypropylene conical vials containing 20 mL of aqueous solutions of Hg(II) or Ni(II) (solution volume (V) = 20 mL) and shaking the vials at 200 rpm in an orbital water bath shaker at a constant temperature (T = 22 ± 3 °C) for certain contact time (t). The solutions were centrifuged at 5000 rpm at the desired contact times to isolate the LDH/MOF NC particles and the supernatant solutions were analyzed using FAAS to measure the residual Hg(II) and Ni(II) concentrations. The pH of the solutions was adjusted with 0.1 mol L^{-1} HCl or 0.1 mol L^{-1} NaOH solutions by using a pH meter throughout the adsorption tests when desired.

Uptake experiments concerning the effect of solution pH on the adsorption efficiency of Hg(II) and Ni(II) were as follows: pH range: 2.0–8.0 for Hg(II) and 3.0–9.0 for Ni(II); initial

metal concentration (C_i) = 25 mg L^{-1}; W = 2.0 mg; V = 20 mL; T = 22 ± 3 °C; t = 120 min; shaking speed = 200 rpm. Uptake experiments concerning the effect of initial concentration were as follows: pH = 3.0 for Hg(II) and pH = 8.0 for Ni(II); C_i = 0.5–250 mg L^{-1}; W = 2.0 mg; V = 20 mL; T = 22 ± 3 °C; t = 120 min; shaking speed = 200 rpm. Uptake experiments concerning the effect of contact time were as follows: pH = 3.0 for Hg(II) and pH = 8.0 for Ni(II); C_i = 100 mg L^{-1}; W = 2.0 mg; V = 20 mL; T = 22 ± 3 °C; t = 1–120 min; shaking speed = 200 rpm. Metal removal percentages and adsorption capacities (Q) were calculated by the following equations:

$$\text{Removal } (\%) = \frac{C_i - C_e}{C_i} \cdot 100 \quad (1)$$

$$Q_t = (C_i - C_t) \cdot \frac{V}{W} \quad (2)$$

$$Q_e = (C_i - C_e) \cdot \frac{V}{W} \quad (3)$$

where C_e, Q_t, and Q_e are the concentration of metal ions at equilibrium (mg L^{-1}), adsorption capacity at any time t (mg g^{-1}), and adsorption capacity at equilibrium (mg g^{-1}), respectively. In order to evaluate and compare the isotherm and kinetic parameters obtained after nonlinear fitting, three statistical parameters including adjusted coefficient of determination ($R^2_{Adj.}$), reduced chi-squared ($X^2_{red.}$), and standard deviation (SD, the root of mean square error) were used. The following equations depict the expression of these statistical parameters (Lima et al., 2015):

$$X^2_{red.} = \sum_i^n \frac{(Q_{i,exp.} - Q_{i,model})^2}{n_p - p} \quad (4)$$

$$SD = \sqrt{\left(\frac{1}{n_p - p}\right) \cdot \sum_i^n (Q_{i,exp.} - Q_{i,model})^2} \quad (5)$$

$$R^2_{Adj.} = 1 - \left(1 - \left[\frac{\sum_i^{n_p} (Q_{i,exp.} - \bar{Q}_{exp})^2 - \sum_i^{n_p} (Q_{i,exp.} - Q_{i,model})^2}{\sum_i^n (Q_{i,exp.} - \bar{Q}_{exp})^2}\right]\right) \cdot \left(\frac{n_p - 1}{n_p - p - 1}\right) \quad (6)$$

where $Q_{i,exp.}$, $Q_{i,model}$, and $\bar{Q}_{exp}$ are each value of Q measured experimentally, each value of Q predicted by the fitted model, and the average of Q experimentally measured, respectively. Also, p and n_p represent the number of parameters of the fitted model and the number of experiments performed, respectively. For the same set of experimental data, the values of $R^2_{Adj.}$, $X^2_{red.}$, and SD are useful to determine the best-fit isotherm and kinetic models.

3. Results and discussion

3.1. Synthesis of LDH/MOF NC

The LDH/MOF NC was synthesized by using a facile and "green" synthesis protocol *via in situ* growth of UiO-66-(Zr)-$(COOH)_2$ nanoparticles on the TA/COOH-$Ni_{50}Co_{50}$-LDH ultrathin sheets. Among the various LDH nanoparticles, Ni_{50}-Co_{50}-LDH was chosen as a scaffold because the strategy used for the preparation of $Ni_{50}Co_{50}$-LDH is an environmentally friendly protocol in which a non-toxic EG-water solvent system is used instead of common toxic and flammable solvents such as dimethylformamide, dimethyl sulfoxide, toluene, acetone, and 1-butanol. Besides, $Ni_{50}Co_{50}$-LDH possesses extended micrometer-size sheets that provide a suitable scaffold for the growth of MOF particles. To date, only a few MOFs have been synthesized under toxic solvent-free conditions (Yang et al., 2013; Sánchez-Sánchez et al., 2015). Among various kind of MOFs, UiO-66-(Zr)-$(COOH)_2$ was chosen because, in addition to good water resistance properties, hydrothermal stability, and the presence of abundant carboxylic groups within its structure as potential adsorption cites, a facile and "green" synthetic method is applied in which water is used as solvent under reflux condition. In order to chemically attach MOF nanoparticles to the LDH sheets, the LDH surface was first chemically functionalized with TASCA and pyromellitic acid molecules. By implementing this strategy, MOF nanoparticles grow chemically on the surface of TA/COOH-LDH sheets due to the presence of abundant carboxylic groups (pyromellitic acid molecules) grafted on the LDH surface. These carboxylic functional groups can act as potential coordination sites for nucleation and growth of clusters in MOF.

Due to the presence of abundant functional groups like —COOH, —NH—, $—NH_2$, —OH, and also aromatic rings in the structure of LDH/MOF NC, this material can be used as a potential adsorbent for the removal of heavy metals. It is reported that among the various kind of functional groups, the —COOH-metal ion interaction is probably the most significant for different applications, especially adsorption (Bala et al., 2007). Fig. 1 displays the overall synthesis procedure for the synthesis of LDH/MOF NC.

3.2. Characterization of the samples

The powder XRD patterns of the samples are shown in Fig. 2. The powder XRD patterns of the pure LDH ($Ni_{50}Co_{50}$-LDH) and the MOF (UiO-66-(Zr)-$(COOH)_2$) exhibited a similar pattern to those observed in previous works (Soltani et al., 2021; Yang et al., 2013; Li et al., 2016), indicating the successful preparation of these samples. The powder XRD profile of the LDH/MOF NC reveals that characteristic peaks representing both MOF and LDH phases are still present in their composite, implying the presence of both phases in the LDH/MOF NC.

FT-IR spectra of the powder samples are shown in Fig. 3. The characteristic absorption bands related to the functional groups of pure $Ni_{50}Co_{50}$-LDH, pure UiO-66-(Zr)-$(COOH)_2$, TA/COOH-LDH, and the LDH/MOF NC were observed and the results are in line with previous reports (Soltani et al., 2021; Yang et al., 2013; Li et al., 2016). For pure Ni_{50}-Co_{50}-LDH, the signal at 1630 cm^{-1} is attributed to the bending vibration of H_2O molecules (interlayer and surface adsorbed water molecules). The FT-IR band at 3445 cm^{-1} is assigned to O-H stretching vibration related to the metal-hydroxyl groups as well as water molecules. The signals at around 1378–1382 cm^{-1} and 2850–2920 cm^{-1} are attributed to the

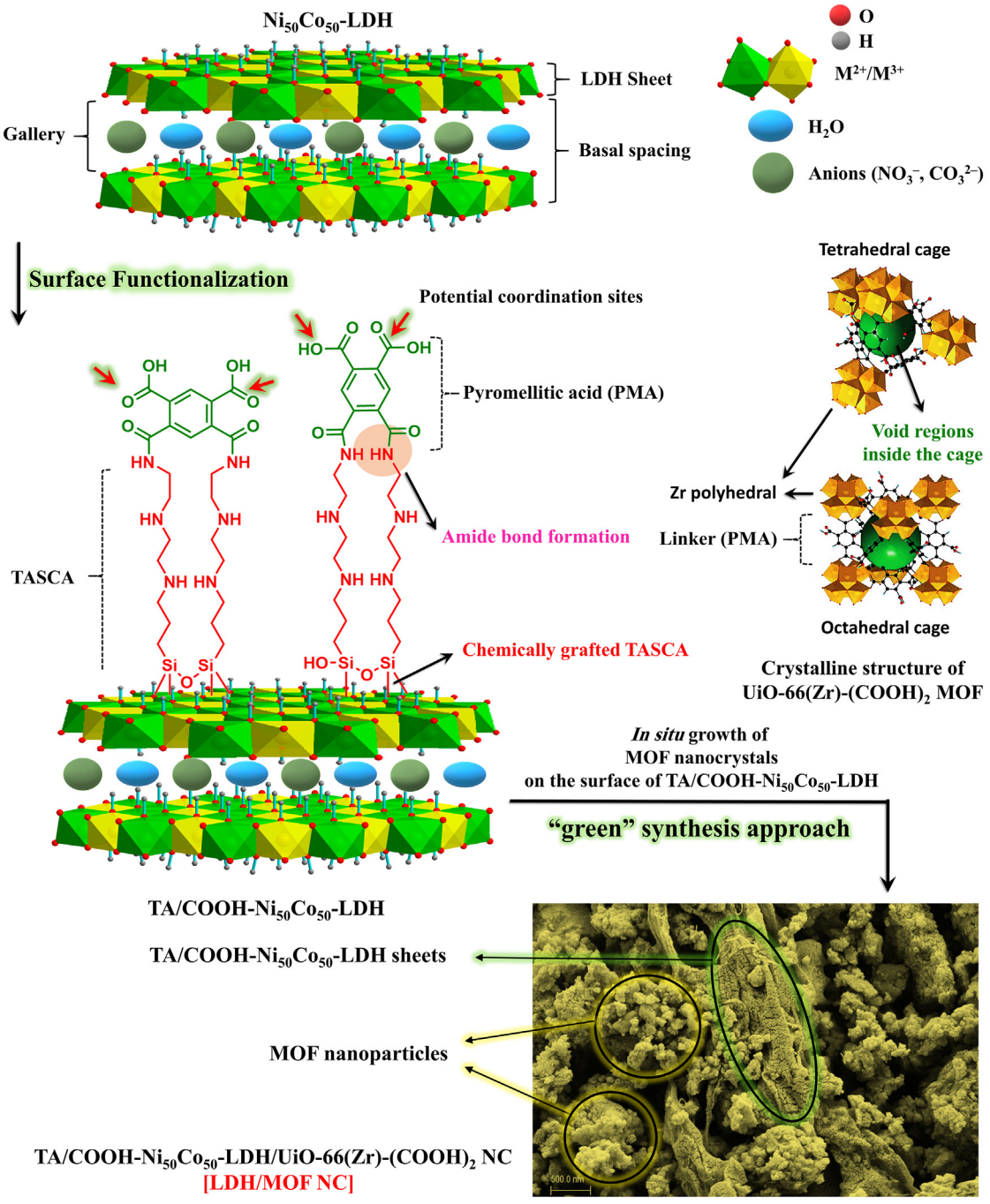

Fig. 1 The overall synthesis process of the LDH/MOF NC.

vibrations of interlayer anions (CO_3^{2-} and NO_3^-) and C—H vibration of trace EG molecules remained in the LDH, respectively. Additionally, the broad absorption band at 632 cm^{-1} is related to the M—O—M, O—M—O, and M—O vibrations (M═Ni and Co). After the surface functionalization, the appearance of new FT-IR signals at 862 cm^{-1},1492 cm^{-1}, and 1570 cm^{-1} are attributed to the aromatic rings of pyromellitic acid molecules. The FT-IR shoulder at 1320–1340 cm^{-1} is attributed to the C—N and C—O stretching modes of carboxyl (—COOH) and amine (—NH_2 and —NH—) groups. Another shoulder at approximately 1640 cm^{-1} is assigned to the amide carbonyls as schematically shown in Fig. 3. In addition, the appearance of a broad signal in the range of 3000–3600 cm^{-1} region is mainly attributed to the carboxyl groups of pyromellitic acid molecules.

Pure UiO-66-(Zr)-$(COOH)_2$ showed two sharp signals with high intensity at 1414 cm^{-1} and 1587 cm^{-1} which related to symmetric and asymmetric stretching vibrations of coordinated carboxylic acid, respectively. The signal at 787 cm^{-1} belongs to the γCH in aromatic rings and absorption bands approximately at 1498 cm^{-1} and 802 cm^{-1} are attributed to vibrational modes of the phenyl rings. The FT-IR band at

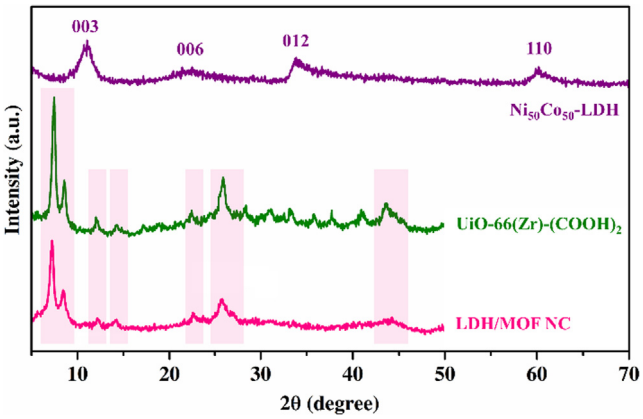

Fig. 2 XRD patterns of the samples.

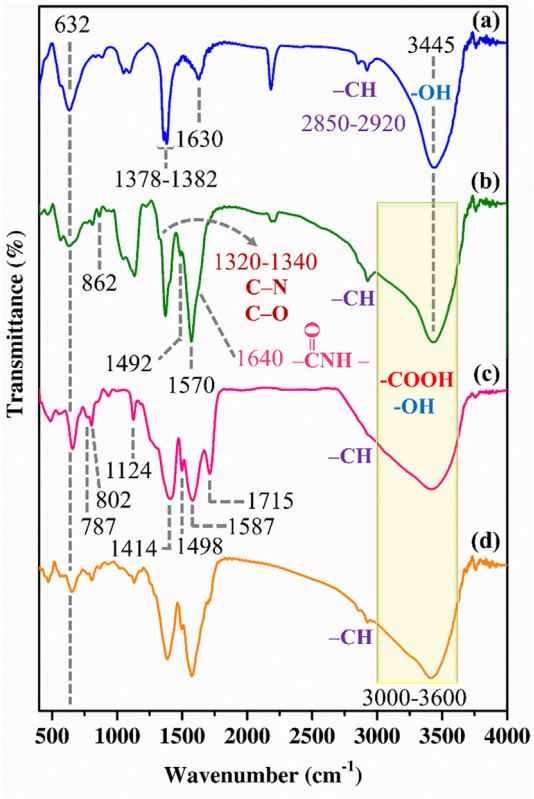

Fig. 3 FT-IR spectra of the $Ni_{50}Co_{50}$-LDH (a), TA/COOH-$Ni_{50}Co_{50}$-LDH (b), UiO-66-(Zr)-$(COOH)_2$ (c), and LDH/MOF NC (d).

1715 cm^{-1} is assigned to the carbonyl group of free carboxylic acid (linker). The broad absorption band in the spectral range of 3400–3600 belongs to acidic OH of free carboxylic groups as well as surface adsorbed water.

FT-IR spectrum of the LDH/MOF NC showed the characteristic absorption bands of both TA/COOH-LDH and UiO-66-(Zr)-$(COOH)_2$, indicating the simultaneous presence of both phases in its structure.

FESEM micrographs of the samples are shown in Fig. 4. The First row of Fig. 4 clearly shows the ultrathin 2D sheets of $Ni_{50}Co_{50}$-LDH. These extended 2D ultrathin sheets can act as a potential scaffold for the growth of various kinds of nanoparticles by implementing an appropriate synthesis strategy. The second row of Fig. 4 reveals the spherical nanoparticles of UiO-66-(Zr)-$(COOH)_2$. The FESEM micrographs taken after *in situ* growth of UiO-66-(Zr)-$(COOH)_2$ nanoparticles on the surface of ultrathin 2D sheets of TA/COOH-$Ni_{50}Co_{50}$-LDH clearly reveal that the nanoparticles are homogeneously distributed on the sheets (Fig. 4, third row). FESEM-EDX mapping analysis of LDH/MOF NC (Fig. 5, the first and second rows) revealed that the synthesized composite possesses a uniform surface structure consisted of a homogeneous distribution of the structural elements (Zr, Ni, Co, O, C, N, Si).

Besides, the EDX peaks corresponding to these elements are depicted in the third row of Fig. 5. The presence of silicon atoms in the structure of the LDH/MOF NC is because of the existence of TASCA molecules in the composite structure (Fig. 1). The origin of nitrogen atoms is also due to the presence of TASCA molecules and interlayer nitrate anions in the gallery space of the $Ni_{50}Co_{50}$-LDH. These observations, in addition to the results of powder XRD and FT-IR analyses, well confirmed the synthesis of the composite through *in situ* growth of the MOF nanoparticles on the surface of the LDH sheets.

In order to gain a better understanding of the textural properties (pore volume and surface area) of the samples, the adsorption–desorption isotherms of the samples were measured at 77 K (Fig. 6). The $Ni_{50}Co_{50}$-LDH reveals a Type III isotherm with a Type H1 hysteresis loop which is representative of the existence of mesopores and macropores (Li et al., 2016). As shown in Fig. 6, both UiO-66-(Zr)-$(COOH)_2$ and LDH/MOF NC reveal a combination of Type IV(a) and Type 1(b) isotherms, which is characteristic of mesoporous and microporous solids, respectively. The characteristic feature of the Type IV isotherm is the presence of a hysteresis loop and Type I(b) isotherm is generally found in solids with possibly narrow mesopores (pore size < 2.5 nm) and micropores (pore size = 1–2 nm) (Thommes et al., 2015). The Brunauer-Emmett-Teller surface area (S_{BET}), the Langmuir surface area ($S_{Langmuir}$), and total pore volume (PV) obtained for all samples are also shown in Fig. 6. It is clear that compared to pure $Ni_{50}Co_{50}$-LDH ($S_{Langmuir} = 27\ m^2\ g^{-1}$ and $PV = 0.23\ cm^3\ g^{-1}$), the LDH/MOF NC possesses a higher surface area and pore volume ($S_{Langmuir} = 69\ m^2\ g^{-1}$ and $PV = 0.35\ cm^3\ g^{-1}$) due to the growth of MOF nanoparticles on the LDH surface. Due to such a bi-/trimodal pore system in the synthesized LDH/MOF NC, the mass transfer through the pores can be dramatically improved (Marjani et al., 2020; Soltani et al., 2020a; Ng et al., 2018). This feature is especially effective in the adsorption, extraction, and catalysis applications where target molecules must reach adsorption sites more quickly.

3.3. Adsorption studies

To evaluate the capability of LDH/MOF NC for the removal of heavy metals, a set of adsorption tests were conducted and some adsorption factors were optimized. Also, several nonlinear isotherm and kinetic models were used to find the plausible adsorption mechanism involved in the removal process. Determining the quality of the fit is achieved by $R^2_{Adj.}$, $X^2_{red.}$, and SD statistics as mentioned before.

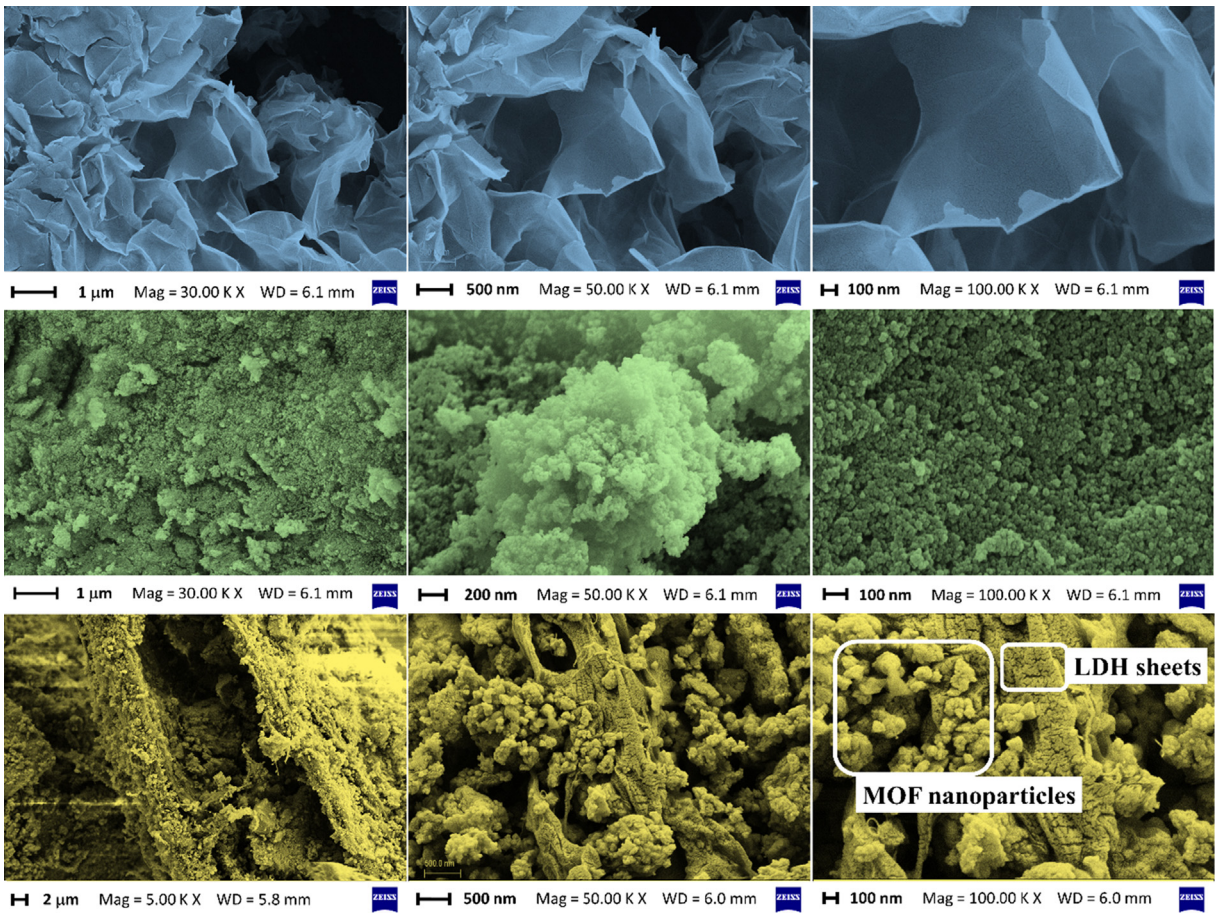

Fig. 4 The FESEM images of pure $Ni_{50}Co_{50}$-LDH (the first row), UiO-66-(Zr)-$(COOH)_2$ (the second row), and LDH/MOF NC (the third row).

The effect of solution pH on the adsorption performance of LDH/MOF NC was investigated (Fig. 7a). For Hg(II), the adsorption rate reached the maximum at the pH value of 3.0 (%Removal ~ 99) and then decreased successively. The lower adsorption rate at pH < 3.0 is due to the high concentration of hydrogen ions (H_3O^+) in the solution and competition with Hg(II) and Ni(II) cations for adsorption sites on the adsorbent surface. At low pHs, the LDH/MOF NC was protonated and the complexation between functional groups of the adsorbent and Hg(II) cations was inhibited because of the electrostatic repulsion between positively charged LDH/MOF NC and Hg(II) cations, leading to a decrease in adsorption rate. Furthermore, it is reported that there would be mercury hydroxide species, $Hg(OH)^+$ or $Hg(OH)_2$, in an aqueous solution when the pH values are more than 3.0 and 4.0 (Fu et al., 2019; Lin et al., 2018), leading to a decrease in adsorption rate. For Ni(II), the maximum removal percentage was observed when the pH value is 8.0. The Ni(II) ion removal pattern for pH changes follows the IMD model (increasing-maximum-decreasing model), which has already been demonstrated by Soltani and co-workers (Soltani et al., 2020e; Soltani et al., 2019). Accordingly, the optimum pH values were 3.0 and 8.0 for adsorption of Hg(II) and Ni(II), respectively, by the LDH/MOF NC from the aqueous solution, and all the next adsorption experiments were carried out under these pH values.

The effect of initial metal ion concentration on the adsorption capacity of the LDH/MOF NC was investigated and the results are shown in Fig. 7b. The adsorption capacities for Hg(II) and Ni(II) continually increase when the initial concentrations of the heavy metals increase from 0.5 mg L^{-1} to 50 mg L^{-1} (the X-axis in Fig. 7b shows the corresponding equilibrium concentrations). The adsorption equilibrium for both Hg(II) and Ni(II) was almost achieved when the initial concentration was 100 mg L^{-1}. After this point, the adsorption capacity for Hg(II) and Ni(II) reached an almost constant value. The experimental maximum adsorption capacities of Hg(II) and Ni (II) by LDH/MOF NC at an initial concentration of 250 mg L^{-1} were 530 mg g^{-1} and 439 mg g^{-1}, respectively. To gain the theoretical maximum adsorption capacity of the adsorbent toward Hg(II) and Ni(II), as well as the plausible adsorption mechanism involved in the adsorption process, three isotherm models, namely the Langmuir (Eq. 7) (Langmuir, 1916), the Freundlich (Eq. 8) (Freundlich, 1906), and the Redlich-Peterson (R-P, Eq. 9) (Redlich and Peterson, 1959), were used. The non-linear form of these equations and their corresponding parameter values after the non-linear fitting method are given in Table 1. Also, the Langmuir, Freundlich, and R-P isotherm curves for adsorption of Hg(II) and Ni(II) ions are shown in Fig. 7b. For the results presented in Table 1, among the two-parameter isotherm models (the Langmuir and the Freundlich), the Langmuir isotherm provides a better fit based

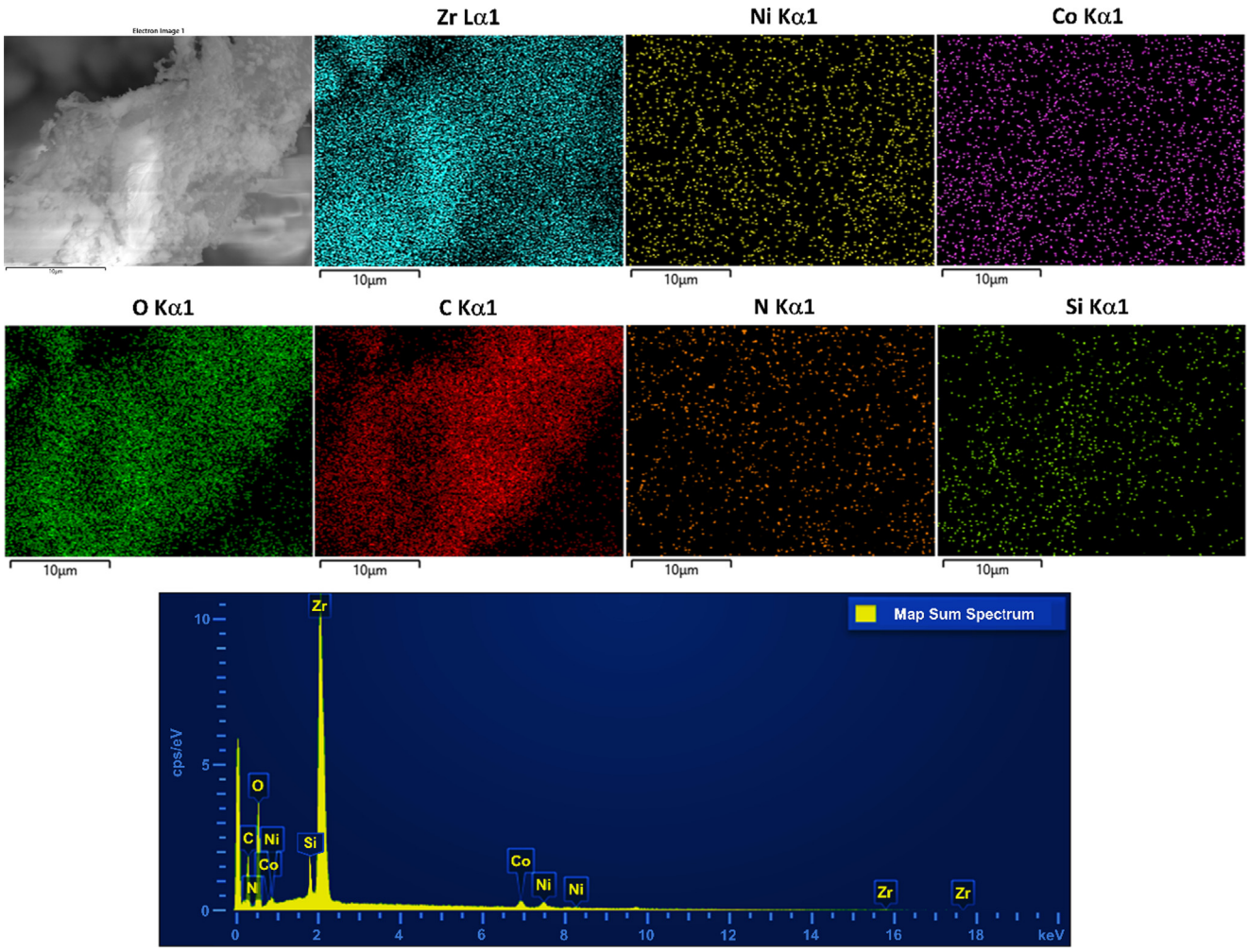

Fig. 5 FESEM-EDX mapping images (the first and second rows) of synthesized LDH/MOF NC adsorbent and the corresponding elements and its EDX spectrum (the third row).

on $R^2_{Adj.}$, $X^2_{red.}$, and SD values. In addition, theoretical maximum adsorption capacities ($Q_{m,cal.}$) of Hg(II) and Ni(II) obtained by the Langmuir equation were close to the corresponding experimental maximum adsorption capacities ($Q_{m,exp.}$) as shown in Table 1.

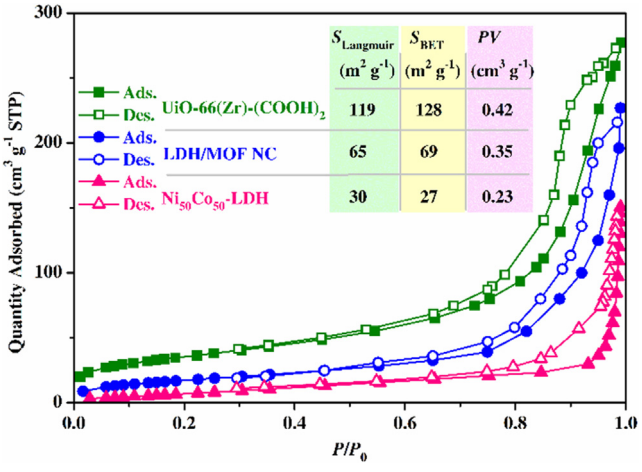

Fig. 6 N_2 adsorption–desorption isotherms of the samples at 77 K and corresponding calculated values for the surface area and the total pore volume.

The R-P model can be applied to ascertain whether the adsorption behavior is the Langmuir or the Freundlich. In this equation, when $g=1$ and $g=0$ the equation reduces to the Langmuir isotherm and becomes linear at low surface coverage, respectively. It was observed that for both Hg(II) and Ni(II) adsorption, the values obtained for exponent ($g=0.9684$ for Hg(II) adsorption and $g=0.9936$ for Ni(II) adsorption) were very close to unity (Table 1), indicating that the adsorption of Hg(II) and Ni(II) ions on the surface of the LDH/MOF NC fits more readily to the Langmuir model than the Freundlich model. Consequently, the adsorption process takes place without any interactions between adsorbates and *via* monomolecular coverage of adsorbate ions on the surface of the LDH/MOF NC adsorbent with a limited number of localized adsorption sites (Lima et al., 2015).

The equilibrium parameter (R_L, Table 1) is a dimensionless factor that can be applied to suggest the adsorption behavior (irreversible as $R_L=0$; unfavorable as $R_L>1$; linear as $R_L=1$; favorable as $0<R_L<1$). The R_L values obtained for Hg(II) and Ni(II) (Table 1) at the highest initial metal concen-

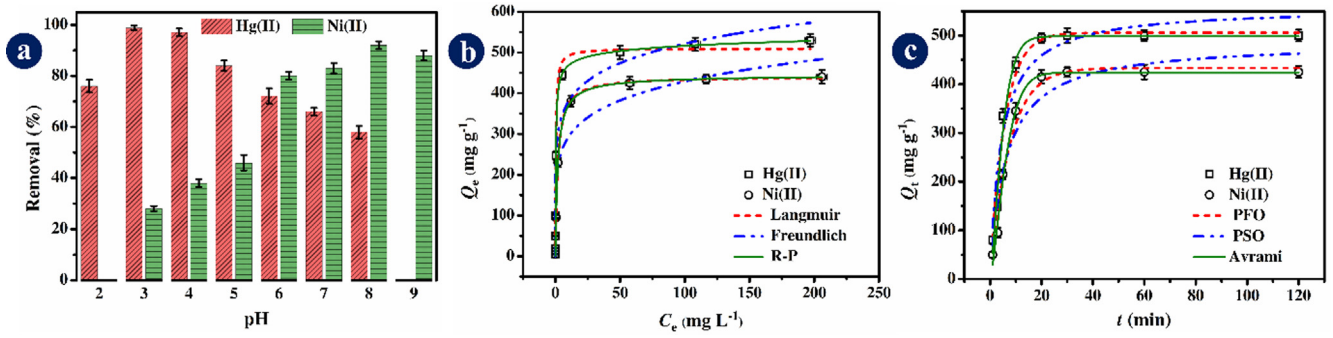

Fig. 7 The effect of pH (a), initial metal concentration (b), and contact time (c) on the adsorption of Hg(II) and Ni(II) by the LDH/MOF NC. The non-linear fitting results for the isotherm and kinetic models are shown in Fig. 7a and Fig. 7b, respectively.

Table 1 Isotherm and kinetic equations and corresponding parameter values and statistics after non-linear fitting method.

				Values			Values	
Eq.	Models	Equations	Parameters[a]	Hg(II)	Ni(II)	Statistics	Hg(II)	Ni(II)
7	Langmuir	$Q_e = \frac{Q_{m,cal.} \cdot K_L \cdot C_e}{1+K_L \cdot C_e}$	$Q_{m,cal.}$	509.8	441.0	$R^2_{Adj.}$	0.9864	0.9885
			K_L	2.771	0.5423	$X^2_{red.}$	720.68	420.83
			R_L	0.001	0.007	SD	26.8	20.5
8	Freundlich	$Q_e = K_F \cdot C_e^{1/n_F}$	K_F	275.8	199.6	$R^2_{Adj.}$	0.9322	0.9254
			n_F	7.23	6.02	$X^2_{red.}$	3596.7	2721.1
						SD	60.0	52.2
9	R-P	$Q_e = \frac{K_{RP} \cdot C_e}{1+\alpha_{RP} \cdot C_e^g}$	K_{RP}	1655	246.5	$R^2_{Adj.}$	0.9887	0.9866
			α_{RP}	3.696	0.5757	$X^2_{red.}$	601.04	488.02
			g	0.9684	0.9936	SD	24.5	22.1
10	PFO	$Q_t = Q_{e,cal.} \cdot (1 - e^{-k_1 \cdot t})$	$Q_{e,cal.}$	505.9	433.4	$R^2_{Adj.}$	0.9695	0.9781
			k_1	0.1786	0.1328	$X^2_{red.}$	891.98	544.88
						SD	29.9	23.3
11	PSO	$Q_t = \frac{k_2 \cdot Q_e^2 \cdot t}{1+Q_e \cdot k_2 \cdot t}$	$Q_{e,cal.}$	557.7	486.4	$R^2_{Adj.}$	0.9203	0.9302
			$k_2 \times 10^{-4}$	4.17	3.37	$X^2_{red.}$	2329.9	1732.7
						SD	48.3	41.6
12	Avrami	$Q_t = Q_{e,cal.} \cdot (1 - e^{(-k_{Av.} \cdot t)^n})$	$Q_{e,cal.}$	498.4	424.1	$R^2_{Adj.}$	0.9767	0.9913
			$k_{Av.}$	0.1908	0.1463	$X^2_{red.}$	682.18	215.69
			n	1.3178	1.3739	SD	26.1	14.7

[a] $Q_{m,cal.}$: theoretical maximum adsorption capacity (mg g^{-1}) assuming a monomolecular layer of adsorbate uptake by the adsorbent, K_L: the Langmuir equilibrium constant (L mg^{-1}); $R_L = [1/(1 + K_L \cdot C_i)]$: separation factor (dimensionless);K_F: the Freundlich equilibrium constant (mg g^{-1}(mg L^{-1})$^{-1/n}$); n_F (the Freundlich exponent (dimensionless); K_{RP} and α_{RP} are Redlich–Peterson isotherm constants with the respective units of (L g^{-1}) and (mg L^{-1})$^{-g}$, respectively; g represents the Redlich–Peterson exponent (dimensionless, $0 < g \leq 1$); $Q_{e,cal.}$: the theoretical equilibrium adsorption capacity (mg g^{-1}); k_1 and k_2 are PFO and PSO rate constants with the respective units of (min^{-1}) and (g mg^{-1} min^{-1}), respectively ; $k_{Av.}$ is the Avrami kinetic constant (min^{-1}); n is a fractional adsorption order (dimensionless) related to the adsorption mechanism.

tration (250 mg L^{-1}) lie between zero and unity, indicating that the adsorption of Hg(II) and Ni(II) by the LDH/MOF NC is favorable.

The effect of contact time on the removal of Hg(II) and Ni (II) by the adsorbent was also investigated and three kinetic models, namely pseudo-first-order (PFO, Eq. 10), pseudo-second-order (PSO, Eq. 11), and Avrami (Eq. 12) were used to fit the experimental adsorption data and to interpret the adsorption behavior.

As shown in Fig. 7c, with increasing contact time from 1 min to 20 min, the adsorption capacity increases sharply, from ~ 80 mg g^{-1} to ~ 500 mg g^{-1} for Hg(II) and from ~ 50 mg g^{-1} to ~ 410 mg g^{-1} for Ni(II), until it reaches almost equilibrium. After 20 min, the adsorption curve reaches a constant state. This relatively rapid adsorption time might be attributed to the presence of abundant adsorption sites (organic functional groups such as —COOH, —NH_2, —NH—, —OH, and aromatic rings) in the adsorbent structure that possesses a high tendency to capture heavy metals from the aqueous medium. The non-linear forms of the three aforementioned kinetic models are given in Table 1. The kinetic parameters after non-linear fitting are also given in Table 1. By comparing the obtained kinetic data after the non-linear fitting method, it can be seen that the Avrami kinetic model gives the best fit to the experimental data than the other two models. The theoretical equilibrium adsorption

capacities ($Q_{e,cal.} = 498.4$ mg g^{-1} for Hg(II) and 424.1 mg g^{-1} for Ni(II)) obtained by the Avrami model are in close agreement with the corresponding experimental adsorption capacities at equilibrium ($Q_{e,exp.} = 500.0$ mg g^{-1} for Hg(II and 425.2 mg g^{-1} for Ni(II)). Also, for both Hg(II) and Ni(II) adsorption, the Avrami model shows a higher $R^2_{Adj.}$ and lower $X^2_{red.}$ and SD values than those parameters obtained by PFO and PSO models.

4. Conclusion

In the present study, we implemented a facile and ''green'' synthesis protocol to prepare the LDH/MOF NC *via* the following three general steps:

(1) Synthesis of ultrathin 2D $Ni_{50}Co_{50}$-LDH sheets without using toxic organic solvents.
(2) Surface functionalization of $Ni_{50}Co_{50}$-LDH sheets with appropriate carboxyl groups with the aim of creating coordination sites to grow the MOF nanoparticles on the functionalized $Ni_{50}Co_{50}$-LDH sheets.
(3) *In situ* formation of MOF nanoparticles on the functionalized $Ni_{50}Co_{50}$-LDH sheets under a simple and effective solvothermal condition at 100 °C and without using toxic organic solvents.

The synthesized samples were characterized by powder XRD, FTIR, FESEM/EDX-mapping, and nitrogen adsorption–desorption analyses. After confirming the structure of LDH/MOF NC by the aforementioned analyses, its adsorption capability for removing Hg(II) and Ni(II) cations from the aqueous medium was investigated. The influence of three adsorption parameters including pH, initial metal concentration, and contact time on the adsorption rate was investigated. Isotherm and kinetic studies were conducted to predict possible adsorption mechanisms involved in the removal process and several nonlinear isotherm and kinetic models were fitted to the experimental data. The theoretical maximum adsorption capacities of Hg(II) and Ni(II) based on the Langmuir model were found to be 509.8 mg g^{-1} and 441.0 mg g^{-1}, respectively, which were in good agreement with corresponding values obtained experimentally (530 mg g^{-1} for Hg(II) and 439 mg g^{-1} for Ni(II) at constant conditions). The high adsorption capacity of the LDH/MOF NC towards Hg(II) and Ni(II) is due to a bi-/trimodal pore system with abundant adsorption sites including —COOH, —NH_2, —NH—, and —OH groups. We believe that the facile and ''green'' synthesis method applied in this work for the synthesis of the LDH/MOF NC can be a starting point for the fabrication and development of similar composite materials for future works, especially for use in applications requiring a material with hierarchical structure and high content of functional groups like —COOH, —NH_2, —NH—, and —OH.

CRediT authorship contribution statement

Roozbeh Soltani: Conceptualization, Methodology, Software, Validation, Formal analysis, Investigation, Writing - original draft, Writing - review & editing, Project administration. **Rasool Pelalak:** Software, Validation. **Mahboubeh Pishnamazi:** Software, Validation, Investigation. **Azam Marjani:** Resources, Supervision, Writing - review & editing. **Saeed Shirazian:** Resources, Validation, Investigation, Supervision, Writing - review & editing, Funding acquisition.

Declaration of Competing Interest

The authors declare that they have no known competing financial interests or personal relationships that could have appeared to influence the work reported in this paper.

Acknowledgements

Saeed Shirazian acknowledges the supports by the Government of the Russian Federation (Act 211, contract 02. A03.21.0011) and by the Ministry of Science and Higher Education of Russia (grant FENU- 2020-0019).

References

Akhtar, N., Iqbal, J., Iqbal, M., 2004. Removal and recovery of nickel (II) from aqueous solution by loofa sponge-immobilized biomass of Chlorella sorokiniana: Characterization studies. J. Hazard. Mater. 108, 85–94. https://doi.org/10.1016/j.jhazmat.2004.01.002.

Azimi, A., Azari, A., Rezakazemi, M., Ansarpour, M., 2017. Removal of heavy metals from industrial wastewaters: A review. ChemBioEng Rev. 4, 37–59. https://doi.org/10.1002/cben.201600010.

Bala, T., Prasad, B.L.V., Sastry, M., Kahaly, M.U., Waghmare, U.V., 2007. Interaction of different metal ions with carboxylic acid group: A quantitative study. J. Phys. Chem. A. 111, 6183–6190. https://doi.org/10.1021/jp067906x.

Bhattacharya, S., Gupta, A.B., Gupta, A., Pandey, A., 2018. Introduction to Water Remediation: Importance and Methods. Springer, Singapore. https://doi.org/10.1007/978-981-10-7551-3_1.

Denkhaus, E., Salnikow, K., 2002. Nickel essentiality, toxicity, and carcinogenicity. Crit. Rev. Oncol. Hematol. 42, 35–56. https://doi.org/10.1016/S1040-8428(01)00214-1.

Feng, M., Zhang, P., Zhou, H.C., Sharma, V.K., 2018. Water-stable metal-organic frameworks for aqueous removal of heavy metals and radionuclides: A review. Chemosphere 209, 783–800. https://doi.org/10.1016/j.chemosphere.2018.06.114.

Freundlich, H.M.F., 1906. Over the adsorption in solution. J. Phys. Chem. 57, 1100–1107.

Fu, F., Wang, Q., 2011. Removal of heavy metal ions from wastewaters: A review. J. Environ. Manage. 92, 407–418. https://doi.org/10.1016/j.jenvman.2010.11.011.

Fu, L., Wang, S., Lin, G., Zhang, L., Liu, Q., Fang, J., Wei, C., Liu, G., 2019. Post-functionalization of UiO-66-NH2 by 2,5-Dimercapto-1,3,4-thiadiazole for the high efficient removal of Hg(II) in water. J. Hazard. Mater. 368, 42–51. https://doi.org/10.1016/j.jhazmat.2019.01.025.

He, X., Qiu, X., Hu, C., Liu, Y., 2018. Treatment of heavy metal ions in wastewater using layered double hydroxides: A review. J. Dispers. Sci. Technol. 39, 792–801. https://doi.org/10.1080/01932691.2017.1392318.

Khajeh, M., Laurent, S., Dastafkan, K., 2013. Nanoadsorbents: Classification, preparation, and applications (with emphasis on aqueous media). Chem. Rev. 113, 7728–7768. https://doi.org/10.1021/cr400086v.

Langmuir, I., 1916. The constitution and fundamental properties of solids and liquids. Part I. Solids. J. Am. Chem. Soc. 38, 2221–2295. https://doi.org/10.1021/ja02268a002.

Li, R., Hu, Z., Shao, X., Cheng, P., Li, S., Yu, W., Lin, W., Yuan, D., 2016. Large scale synthesis of NiCo layered double hydroxides for superior asymmetric electrochemical capacitor. Sci. Rep. 6, 1–9. https://doi.org/10.1038/srep18737.

Liang, X., Zang, Y., Xu, Y., Tan, X., Hou, W., Wang, L., Sun, Y., 2013. Sorption of metal cations on layered double hydroxides. Colloids Surfaces A Physicochem. Eng. Asp. 433, 122–131. https://doi.org/10.1016/j.colsurfa.2013.05.006.

Lima, É.C., Adebayo, M.A., Machado, F.M., 2015. Kinetic and equilibrium models of adsorption. In: Carbon Nanostructures. Springer, Cham. https://doi.org/10.1007/978-3-319-18875-1_3.

Lin, G., Wang, S., Zhang, L., Hu, T., Peng, J., Cheng, S., Fu, L., 2018. Selective and high efficient removal of Hg^{2+} onto the functionalized corn bract by hypophosphorous acid. J. Clean. Prod. 192, 639–646. https://doi.org/10.1016/j.jclepro.2018.05.043.

Marjani, A., Soltani, R., Pishnamazi, M., Rezakazemi, M., Shirazian, S., 2020. Functionalized pollen-like mesoporous silica. Microporous Mesoporous Mater. 310, 110531. https://doi.org/10.1016/j.micromeso.2020.110531.

Ng, S.W.L., Yilmaz, G., Ong, W.L., Ho, G.W., 2018. One-step activation towards spontaneous etching of hollow and hierarchical porous carbon nanospheres for enhanced pollutant adsorption and energy storage. Appl. Catal. B Environ. 220, 533–541. https://doi.org/10.1016/j.apcatb.2017.08.069.

Redlich, O., Peterson, D.L., 1959. A useful adsorption isotherm. J. Phys. Chem. 63, 1024. https://doi.org/10.1021/j150576a611.

Sánchez-Sánchez, M., Getachew, N., Díaz, K., Díaz-García, M., Chebude, Y., Díaz, I., 2015. Synthesis of metal-organic frameworks in water at room temperature: Salts as linker sources. Green Chem. 17, 1500–1509. https://doi.org/10.1039/c4gc01861c.

Soltani, R., Marjani, A., Shirazian, S., 2019. Facile one-pot synthesis of thiol-functionalized mesoporous silica submicrospheres for Tl(I) adsorption: Isotherm, kinetic and thermodynamic studies. J. Hazard. Mater. 371, 146–155. https://doi.org/10.1016/j.jhazmat.2019.02.076.

Soltani, R., Marjani, A., Shirazian, S., 2019. Shell-in-shell monodispersed triamine-functionalized SiO_2 hollow microspheres with micro-mesostructured shells for highly efficient removal of heavy metals from aqueous solutions. J. Environ. Chem. Eng. 7, 102832. https://doi.org/10.1016/j.jece.2018.102832.

Soltani, R., Marjani, A., Shirazian, S., 2020a. A hierarchical LDH/MOF nanocomposite: Single, simultaneous and consecutive adsorption of a reactive dye and Cr(vi). Dalt. Trans. 49, 5323–5335. https://doi.org/10.1039/d0dt00680g.

Soltani, R., Marjani, A., Hosseini, M., Shirazian, S., 2020b. Synthesis and characterization of novel N-methylimidazolium-functionalized KCC-1: A highly efficient anion exchanger of hexavalent chromium. Chemosphere 239, 124735. https://doi.org/10.1016/j.chemosphere.2019.124735.

Soltani, R., Marjani, A., Hosseini, M., Shirazian, S., 2020c. Mesostructured hollow siliceous spheres for adsorption of dyes. Chem. Eng. Technol. 43, 392–402. https://doi.org/10.1002/ceat.201900470.

Soltani, R., Marjani, A., Soltani, R., Shirazian, S., 2020d. Hierarchical multi-shell hollow micro–meso–macroporous silica for Cr(VI) adsorption. Sci. Rep. 10, 1–12. https://doi.org/10.1038/s41598-020-66540-6.

Soltani, R., Pishnamazi, M., Pelalak, R., Rezakazemi, M., Marjani, A., Dinari, M., Sarkar, S.M., Shirazian, S., 2020e. Preparation of COOH-KCC-1/polyamide 6 composite by in situ ring-opening polymerization: synthesis, characterization, and Cd(II) adsorption study. J. Environ Chem. Eng., 104683 https://doi.org/10.1016/j.jece.2020.104683.

Soltani, R., Marjani, A., Hosseini, M., Shirazian, S., 2020f. Meso-architectured siliceous hollow quasi-capsule. J. Colloid Interface Sci. 570, 390–401. https://doi.org/10.1016/j.jcis.2020.03.003.

Soltani, R., Pelalak, R., Pishnamazi, M., Marjani, A., Albadarin, A.B., Sarkar, S.M., Shirazian, S., 2021. A novel and facile green synthesis method to prepare LDH/MOF nanocomposite for removal of Cd (II) and Pb (II). Sci. Rep. 11, 1–15. https://doi.org/10.1038/s41598-021-81095-w.

Thommes, M., Kaneko, K., Neimark, A.V., Olivier, J.P., Rodriguez-Reinoso, F., Rouquerol, J., Sing, K.S.W., 2015. Physisorption of gases, with special reference to the evaluation of surface area and pore size distribution (IUPAC Technical Report). Pure Appl. Chem. 87, 1051–1069. https://doi.org/10.1515/pac-2014-1117.

Wen, J., Fang, Y., Zeng, G., 2018. Progress and prospect of adsorptive removal of heavy metal ions from aqueous solution using metal–organic frameworks: A review of studies from the last decade. Chemosphere 201, 627–643. https://doi.org/10.1016/j.chemosphere.2018.03.047.

Yang, Q., Vaesen, S., Ragon, F., Wiersum, A.D., Wu, D., Lago, A., Devic, T., Martineau, C., Taulelle, F., Llewellyn, P.L., Jobic, H., Zhong, C., Serre, C., De Weireld, G., Maurin, G., 2013. A water stable metal-organic framework with optimal features for CO_2 capture. Angew. Chemie - Int. Ed. 52, 10316–10320. https://doi.org/10.1002/anie.201302682.

Zahir, F., Rizwi, S.J., Haq, S.K., Khan, R.H., 2005. Low dose mercury toxicity and human health. Environ. Toxicol. Pharmacol. 20, 351–360. https://doi.org/10.1016/j.etap.2005.03.007.